

CrossMark  
click for updatesCite this: *J. Mater. Chem. A*, 2017, 5,  
925Received 29th October 2016  
Accepted 5th December 2016

DOI: 10.1039/c6ta09360d

www.rsc.org/MaterialsA

## An intercalated graphene/(molybdenum disulfide) hybrid fiber for capacitive energy storage†

Bingjie Wang,‡ Qingqing Wu,‡ Hao Sun, Jing Zhang, Jing Ren, Yongfeng Luo,  
Min Wang\* and Huisheng Peng\*

It is critical but remains challenging to make fiber-shaped energy storage systems to satisfy the rapidly developing area of flexible and wearable electronics due to the difficulty in finding high-performance fiber electrodes. Herein, we designed a one-step hydrothermal strategy to synthesize graphene/(molybdenum disulfide) hybrid fiber electrodes with a novel intercalated nanostructure that effectively combined the high electrical conductivity from graphene sheets and high pseudocapacitance from molybdenum disulfide sheets. The intercalated nanostructure also simultaneously provided large ion-accessible surface areas and a high active material content of up to 33.98 wt%. The resulting fiber-shaped supercapacitor exhibited a high specific capacitance of  $368 \text{ F cm}^{-3}$ .

The rapid development of next-generation electronics such as wearable devices has prompted the exploration of matching power accessories with high flexibility and portability.<sup>1–3</sup> To this end, fiber-shaped energy harvesting and storage devices have attracted much attention in recent years due to their exhibited high flexibility, portability and wearability.<sup>4,5</sup> Among them, fiber-shaped supercapacitors have been considered as promising candidates for future wearable power devices.<sup>6–10</sup> However, the energy storage performances of the reported fiber-shaped supercapacitors are generally much lower compared with their planar counterparts as it is not easy to find high-performance fiber electrodes.<sup>8,11,12</sup> The challenge lies in the efficient incorporation of active materials into conducting skeletons, for which a balance should be struck to enhance active material loading while maintaining the electrical conductivity to the greatest extent.<sup>13–15</sup> Meanwhile, several methods have been attempted to improve the mechanical properties of hybrid materials, including borate cross-linking,<sup>16</sup> grafting with

$\pi$ -conjugated molecules or polymers,<sup>17,18</sup> and layer-to-layer reinforcement.<sup>19</sup> However, it remains a challenge to reach the above goal due to the high stacking trend of widely studied nanomaterials, which largely hinders their practical applications.

Herein, we designed a one-step hydrothermal strategy to prepare graphene/molybdenum disulfide ( $\text{MoS}_2$ ) hybrid fibers with a novel intercalated nanostructure. The reduction of graphene oxide (GO) and the growth of  $\text{MoS}_2$  were simultaneously achieved during the hydrothermal process, which avoided negative effects on the pseudocapacitive materials during the chemical reduction process. Large graphene sheets formed a robust skeleton intercalated by small  $\text{MoS}_2$  sheets filling the spaces and microvoids in the hybrid fiber (Fig. 1a). The graphene sheets offered continuous pathways for electron transport and ideal platforms for the epitaxial growth of  $\text{MoS}_2$  sheets (Fig. 1b). The designed intercalated nanostructure also simultaneously provided large ion-accessible surface areas and a high active material content of up to 33.98 wt%. When the hybrid fiber was used as an electrode, the fiber-shaped supercapacitor demonstrated a high specific capacitance of  $368 \text{ F cm}^{-3}$  at  $0.1 \text{ A cm}^{-3}$ .

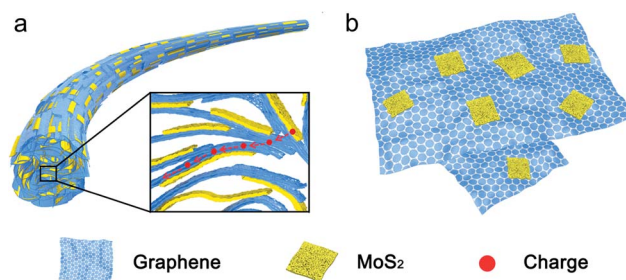


Fig. 1 (a) Schematic illustration of the intercalated nanostructure of the graphene/ $\text{MoS}_2$  hybrid fiber. The transport pathways that are indicated by the arrows are used to emphasize the interaction between graphene and  $\text{MoS}_2$  layers. (b) Schematic illustration of the epitaxial growth of small  $\text{MoS}_2$  sheets on large graphene sheets.

State Key Laboratory of Molecular Engineering of Polymers, Department of Macromolecular Science, Laboratory of Advanced Materials, Fudan University, Shanghai 200438, China. E-mail: minwang@fudan.edu.cn; penghs@fudan.edu.cn

† Electronic supplementary information (ESI) available. See DOI: 10.1039/c6ta09360d

‡ These authors contributed equally to this work.

The synthesis of the graphene/MoS<sub>2</sub> hybrid fiber is illustrated in Fig. S1†. In brief, a mixed solution containing (NH<sub>4</sub>)<sub>2</sub>MoS<sub>4</sub> and GO was injected into a polytetrafluoroethylene (PTFE) tube (Fig. S2a†). After being sealed at the two ends, the tube was heated and kept at 220 °C to prepare the graphene/MoS<sub>2</sub> hybrid fiber *via* a hydrothermal method (Fig. S2b†). The as-prepared hybrid fiber in water shared a similar diameter of ~300 μm with a bare graphene fiber prepared *via* the same method, and rapidly shrank to 80 μm after drying in air in 90 s (Fig. S3†). The graphene/MoS<sub>2</sub> hybrid fiber can be scaled up by increasing the length of the PTFE tube (Fig. S4†). The MoS<sub>2</sub> in the hybrid fiber was further verified using X-ray photoelectron spectroscopy and X-ray diffraction (Fig. S5 and S6†).

The graphene/MoS<sub>2</sub> hybrid fiber exhibited a porous structure at low magnification (Fig. 2a), and small MoS<sub>2</sub> sheets (black stripes) were uniformly distributed along the direction of the layered graphene, which showed an intercalated nanostructure between the graphene and MoS<sub>2</sub> sheets (Fig. 2b). These hybrid fibers were different from wet-spun graphene fibers made by incorporating functional components such as bismuth oxide nanotubes<sup>20</sup> and MoS<sub>2</sub> (ref. 21) into GO solutions. Large graphene sheets not only served as promising platforms for the growth of thin MoS<sub>2</sub> sheets, but also inhibited the aggregation of MoS<sub>2</sub> sheets (Fig. S7†). An interlayer spacing of 0.63 nm that corresponded to the MoS<sub>2</sub> sheets was calculated from the transmission electron microscopy image (Fig. 2c).<sup>22</sup>

At a low MoS<sub>2</sub> content of 9.91 wt%, large graphene sheets were clearly observed (Fig. 2d), and small MoS<sub>2</sub> sheets grew on the surface of the graphene sheets with average lateral sizes of 5–10 nm. Selected area electron diffraction images showed that the graphene sheet in the hybrid fiber was different from the typical hexagonal symmetry of bare graphene sheets (Fig. S8†).<sup>23</sup> The bright spots correspond to the diffractions from graphene, and the bright circles are derived from randomly distributed MoS<sub>2</sub> sheets, where the inner and external ones represent MoS<sub>2</sub> (100) and MoS<sub>2</sub> (110) reflections, respectively.<sup>24</sup> With the increasing MoS<sub>2</sub> content, ultrathin and small layered MoS<sub>2</sub> sheets grew into thicker and larger sheets with uniform distribution, which were partially overlapped with each other. For

instance, flower-like MoS<sub>2</sub> sheets were decorated on graphene sheets with a content of 17.04 wt% (Fig. 2e). A further increase such as to 33.98 wt% led to a more uniform distribution of MoS<sub>2</sub> sheets on the graphene surfaces (Fig. 2f). This intercalated nanostructure enhanced the interfaces between the graphene and MoS<sub>2</sub> sheets and contributed to high electrochemical properties, which will be discussed later.

Graphene/MoS<sub>2</sub> hybrid fibers with different MoS<sub>2</sub> amounts exhibited different morphologies (Fig. 3). For a bare graphene fiber, the highly wrinkled surface was produced by a drastic shrinkage of the graphene sheets during water evaporation (Fig. 3a), and a porous surface consisting of loosely stacked graphene sheets was observed (Fig. 3b). The cross-sectional scanning electron microscopy (SEM) image showed that the network was formed by layered graphene sheets with abundant voids in the fiber (Fig. 3c). At low MoS<sub>2</sub> amounts such as 2.06 wt%, the hybrid fiber shared a similar morphology with the bare graphene fiber (Fig. S9†). However, when the content increased to 17.04 wt%, the hybrid fiber showed a more compact surface and uniform diameter (Fig. 3d), and the alignment of the graphene sheets along the length direction became better (Fig. 3e). As seen in the cross-sectional SEM image, more small MoS<sub>2</sub> sheets are intercalated among large graphene sheets (Fig. 3f). These hybrid fibers show different morphologies from the wet-spun graphene/MoS<sub>2</sub> fiber (Fig. S10†). With the increasing MoS<sub>2</sub>, the high degree of orientation and densely stacked intercalated structure of the hybrid fiber has been well maintained (Fig. S11†), even at a MoS<sub>2</sub> content of 33.98 wt% (Fig. 3g–i). The above phenomenon can be explained by the shrinking of graphene sheets during the drying process. For instance, the shrinkage ratios of the hybrid fiber increased from 60.2% to 79.2% when the MoS<sub>2</sub> content increased from 2.06 wt% to 33.98 wt% (Fig. S12†). A higher shrinkage ratio increased the alignment and compactness of the graphene sheets under drying.

The addition of guest components decreased the formation of the liquid crystal structure for GO solutions, which in turn reduced their spinability.<sup>25</sup> As a result, the content of the functional components was lower for wet-spun graphene/MoS<sub>2</sub>

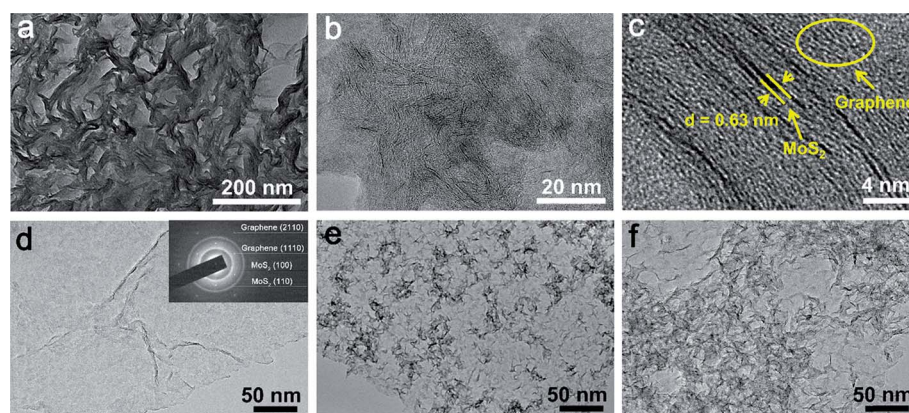


Fig. 2 (a–c) TEM images of the axial cross section of the graphene/MoS<sub>2</sub> hybrid fiber (MoS<sub>2</sub> content of 17.04 wt%). (d–f) TEM images of the graphene/MoS<sub>2</sub> hybrids with increasing MoS<sub>2</sub> content (d, 9.91 wt%; e, 17.04 wt%; f, 33.98 wt%).

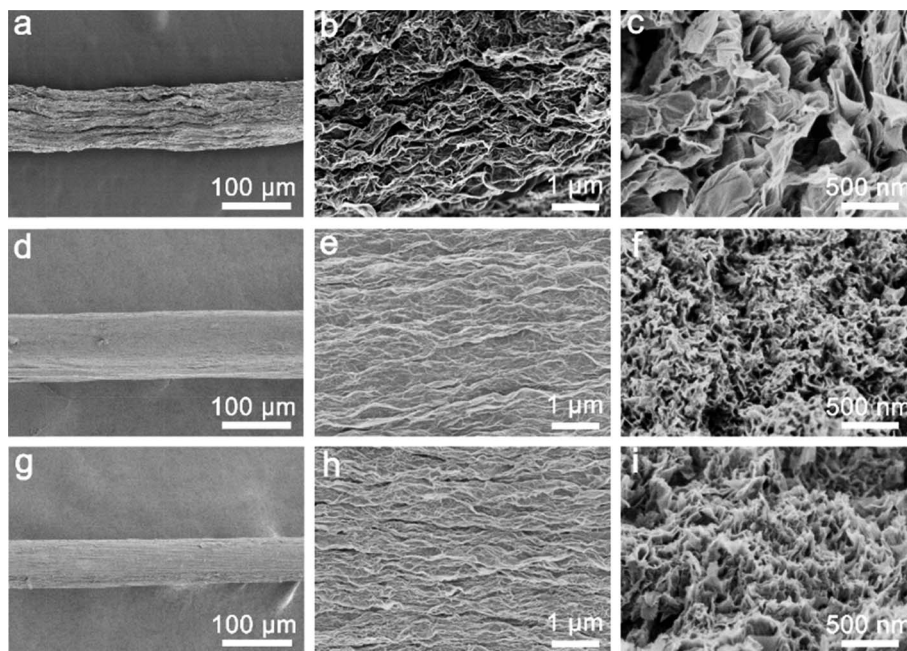


Fig. 3 SEM images of bare graphene (a–c) and hybrid graphene/MoS<sub>2</sub> fibers with a MoS<sub>2</sub> content of 17.04 wt% (d–f) and 33.98 wt% (g–i) at low magnification (a, d and g), high magnification by side view (b, e and h) and high magnification by top view (c, f and i).

hybrid fibers, *e.g.* up to 2.02 wt% in previous work.<sup>21</sup> In contrast, here the MoS<sub>2</sub> content reached 33.98 wt%, which was verified using thermogravimetric analysis (Fig. S13†).<sup>26</sup> Note that a further increase in the MoS<sub>2</sub> content could not form continuous hybrid fibers after the hydrothermal process (Fig. S14†), and the aligned graphene sheets evolved into a randomly stacked structure (Fig. S15†). Too many MoS<sub>2</sub> sheets destroyed the continuous and oriented assembly of the graphene sheets.

The graphene/MoS<sub>2</sub> hybrid sheets shrank in air to form an intercalated nanostructure similar to bare graphene fibers.<sup>27</sup> However, different from the porous transverse section in a bare graphene fiber (Fig. 4a), small MoS<sub>2</sub> sheets filled in the voids among the graphene sheets and formed a denser structure (Fig. 4b). As a result, the hybrid fiber exhibited higher densities with increasing MoS<sub>2</sub> content, *e.g.*, from ~0.76 to ~1.72 g cm<sup>-3</sup> when the content increased from 0 to 33.98 wt% (Fig. 4c). This dense intercalated nanostructure was also beneficial for promoting the mechanical properties of the hybrid fiber.<sup>28</sup> The tensile strength reached 294 MPa at a MoS<sub>2</sub> content of 17.04 wt% and it had been increased by 112% compared with bare graphene fibers under the same conditions (Fig. 4d). A further increase of the MoS<sub>2</sub> content led to a reduction in the strength, which was mainly ascribed to the disruption of the graphene skeleton with a large amount of small MoS<sub>2</sub> sheets. The decrease of the elongation also revealed an increase in the brittleness of the hybrid fibers at higher MoS<sub>2</sub> amounts (Fig. S16†).<sup>29</sup> However, even for a high content of 33.98 wt%, a tensile strength of 181 MPa was obtained compared with 138 MPa for a bare graphene fiber. The hybrid fiber was flexible and could be made into a knot (Fig. S17†) or woven into textiles without damaging its structure (Fig. S18†). The design of a continuous fabrication

process with a shorter hydrothermal reaction aiming at large-scale production is underway.

Due to the formation of continuous conducting pathways by the graphene sheets, the hybrid fibers were electrically conductive and were comparable with bare graphene fibers in conductivity (Fig. S19†).<sup>27</sup> Two hybrid fibers were separately deposited with an electrolyte layer based on a solution process and then used as parallel electrodes to produce a fiber-shaped supercapacitor. The electrolyte thickness had little effect on the capacitance,<sup>30</sup> and a thickness of ~10 μm was mainly used here due to the easy preparation.

The intercalated nanostructure efficiently combined the advantages of graphene and MoS<sub>2</sub> such as high electrical conductivity and high electrochemical activity, respectively. The electrochemical properties of bare graphene and graphene/MoS<sub>2</sub> hybrid fibers were compared using cyclic voltammetry (CV) at a scan rate of 5 mV s<sup>-1</sup> in a three-electrode system. A typical pseudocapacitive behavior of the hybrid fiber was confirmed by the reversible cathodic and anodic peaks from the CV curves (Fig. 5a), and the hybrid fibers with higher MoS<sub>2</sub> amounts exhibited much higher current densities in the CV curves due to the greater pseudocapacitance contribution from MoS<sub>2</sub>. The galvanostatic charge–discharge curves of the fiber-shaped supercapacitor containing two graphene/MoS<sub>2</sub> hybrid fibers shared a triangular shape with different amounts of MoS<sub>2</sub> (Fig. 5b). The volumetric specific capacitances increased with increasing MoS<sub>2</sub> amounts (Fig. 5c), and a maximal specific capacitance of 368 F cm<sup>-3</sup> (area specific capacitance: 598 mF cm<sup>-2</sup>) was achieved at 33.98 wt%. Note that the capacitance of supercapacitors is mainly derived from the surface reactions of electrode materials, including charge separation at electrode/electrolyte interfaces and the faradic redox reaction, which

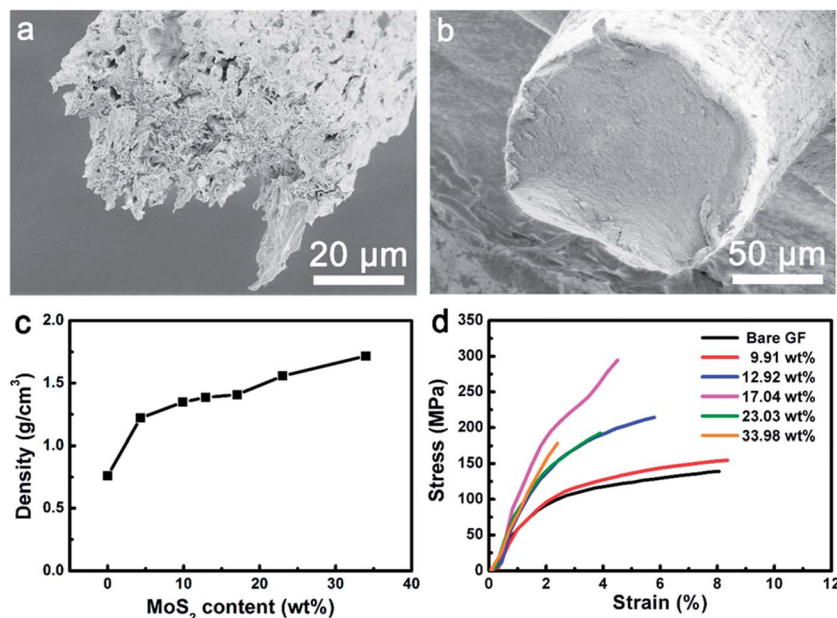


Fig. 4 (a and b) Cross-sectional SEM images of bare graphene and graphene/MoS<sub>2</sub> hybrid (MoS<sub>2</sub> content of 33.98 wt%) fibers, respectively. (c) Dependence of density on the MoS<sub>2</sub> content of the hybrid fiber. (d) Stress–strain curves of bare graphene and graphene/MoS<sub>2</sub> hybrid fibers with increasing weight amounts.

occurred on the surfaces and were not controlled by the ion diffusion process.<sup>31</sup> Due to the voids in the hybrid fiber, electrolyte can slowly infiltrate the hybrid fiber, which enhanced the contact between electrolyte and electrode. As a result, the performance can be well maintained during charging and discharging at a high current density.

Importantly, the fiber-shaped supercapacitor based on the graphene/MoS<sub>2</sub> fiber can normally charge and discharge at high current densities (Fig. S20†). The mass specific capacitance increased with the increasing MoS<sub>2</sub> content when the weight content was less than 23.03 wt% (248 F g<sup>-1</sup> for 23.03 wt%) (Fig. S21†). Upon further increasing the MoS<sub>2</sub> to 33.98 wt%, the mass specific capacitance decreased to 214 F g<sup>-1</sup>, indicating a low utilization rate of MoS<sub>2</sub> sheets. The rise of the volumetric specific capacitance was attributed to the increasing densities of the hybrid fibers. A high cycling stability was verified by tracing the capacitance variation during 8000 charge–discharge cycles (Fig. 5d). The mass specific capacitances at different current densities revealed high electrochemical performances (Fig. S22†). The as-fabricated fiber-shaped supercapacitors inherited the good strength and flexibility of the hybrid fibers, demonstrating highly overlapped CV curves under deformation (Fig. S23†) and dependence of the capacitance on bending number (Fig. S24†).

The fiber-shaped supercapacitors based on graphene/MoS<sub>2</sub> hybrid fibers displayed the highest volumetric specific capacitance compared with previous reports (Fig. 5e).<sup>7,11–13,15,25,32,33</sup> The one-step hydrothermal process here could realize much higher amounts of MoS<sub>2</sub>, which contributed to capacitance enhancement of the resulting supercapacitors. Moreover, the intercalated nanostructure formed between the graphene and MoS<sub>2</sub> sheets efficiently increased their contacts to effectively

incorporate the high pseudocapacitances of MoS<sub>2</sub> sheets and the rapid conducting pathways from graphene sheets during charging and discharging.

In summary, a one-step hydrothermal strategy was designed to synthesize graphene/MoS<sub>2</sub> hybrid fibers for fiber-shaped supercapacitors. The novel intercalated nanostructure effectively combined the high electrical conductivity from graphene sheets and high pseudocapacitance from MoS<sub>2</sub> sheets. These fiber-shaped supercapacitors exhibited the highest specific capacitance of 368 F cm<sup>-3</sup> among the available reports. This work also represents a general and effective strategy for the development of high-performance hybrid electrode materials and devices.

## Experimental section

### Synthesis of graphene/MoS<sub>2</sub> hybrid fibers

GO was synthesized *via* a modified Hummer's method. Poly(vinyl pyrrolidone) (34 mg) (*M<sub>w</sub>* of 40 000) was added to deionized water (70 mL) under vigorous stirring for 1 h, followed by the addition of (NH<sub>4</sub>)<sub>2</sub>MoS<sub>4</sub> (137 mg), stirring for 2 h, ultrasonic treatment for 2 h and vigorous stirring overnight to produce a homogeneous precursor solution (2 mg mL<sup>-1</sup>). GO/(NH<sub>4</sub>)<sub>2</sub>MoS<sub>4</sub> aqueous dispersions with different mass ratios were prepared by mixing a (NH<sub>4</sub>)<sub>2</sub>MoS<sub>4</sub> precursor solution (2 mg mL<sup>-1</sup>), GO aqueous solution (2 mg mL<sup>-1</sup>) and deionized water, followed by ultrasonic treatment and stirring for 0.5 and 2 h, respectively. The obtained dispersion was further concentrated to ~10 mg mL<sup>-1</sup> and injected into a polytetrafluoroethylene (PTFE) tube (inner diameter, 0.5 mm). The tube was sealed at both ends and placed in an autoclave which served as a hydrothermal reactor, followed by heating in a muffle furnace at

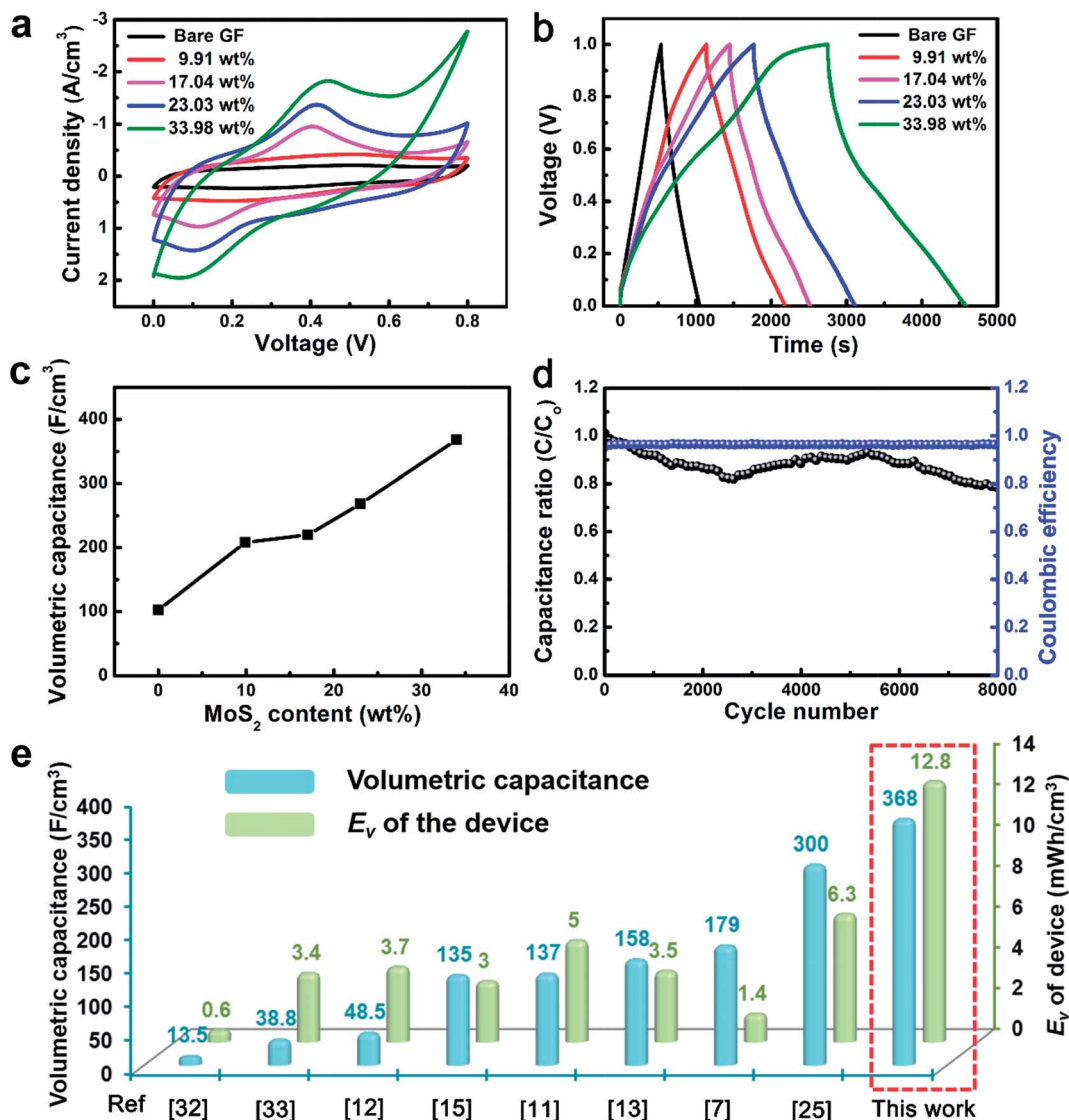


Fig. 5 (a) CV curves of graphene/MoS<sub>2</sub> hybrid fibers with different amounts of MoS<sub>2</sub> at 5 mV s<sup>-1</sup> in 1 M H<sub>2</sub>SO<sub>4</sub>. (b) Galvanostatic charge-discharge curves of fiber-shaped supercapacitors prepared from graphene/MoS<sub>2</sub> hybrid fibers with different amounts of MoS<sub>2</sub>. The current density for charge and discharge was 0.1 A cm<sup>-3</sup>. (c) Dependence of volumetric capacitance on the MoS<sub>2</sub> content in the supercapacitor. (d) Cycling performance of the supercapacitor based on the graphene/MoS<sub>2</sub> hybrid fiber electrode. (e) Comparison of the supercapacitor based on the graphene/MoS<sub>2</sub> fiber with other reports in terms of volumetric capacitance and energy density.

220 °C for 6 h. After cooling down to room temperature, the graphene/MoS<sub>2</sub> hybrid fiber was pushed out by water flow (~0.5 m s<sup>-1</sup>). Here water was used due to the convenience in operation. The obtained hybrid fibers were then dried in air for 2 h.

### Fabrication of the fiber-shaped supercapacitors

Firstly, a polymer gel electrolyte was prepared. 1 g of PVA was added to 9 g of deionized water and then swollen for 3 h at room temperature, followed by heating at 90 °C for 15 min and addition of 1.1 g of H<sub>3</sub>PO<sub>4</sub>. One graphene/MoS<sub>2</sub> hybrid fiber was coated with a uniform layer of gel electrolyte on the surface. The same two modified hybrid fibers were placed in parallel to make a fiber-shaped supercapacitor.

### Acknowledgements

This work was supported by MOST (2016YFA0203302), NSFC (21634003, 51573027, 51403038, 51673043, 21604012, 21474017) and STCSM (16JC1400702, 15XD1500400, 15JC1490200).

### References

- W. Weng, P. N. Chen, S. S. He, X. M. Sun and H. S. Peng, *Angew. Chem., Int. Ed.*, 2016, 55, 6140–6169.
- L. Li, Z. Wu, S. Yuan and X. B. Zhang, *Energy Environ. Sci.*, 2014, 7, 2101–2122.
- G. Zhou, F. Li and H. M. Cheng, *Energy Environ. Sci.*, 2014, 7, 1307–1338.

- 4 Y. Zhang, Y. Zhao, J. Ren, W. Weng and H. S. Peng, *Adv. Mater.*, 2016, **28**, 4524–4531.
- 5 D. S. Yu, Q. Qian, L. Wei, W. C. Jiang, K. L. Goh, J. Wei, J. Zhang and Y. Chen, *Chem. Soc. Rev.*, 2015, **44**, 647–662.
- 6 B. J. Wang, X. Fang, H. Sun, S. S. He, J. Ren, Y. Zhang and H. S. Peng, *Adv. Mater.*, 2015, **27**, 7854–7860.
- 7 J. A. Lee, M. K. Shin, S. H. Kim, H. U. Cho, G. M. Spinks, G. G. Wallace, M. D. Lima, X. Lepró, M. E. Kozlov, R. H. Baughman and S. J. Kim, *Nat. Commun.*, 2013, **4**, 1970.
- 8 Y. N. Meng, Y. Zhao, C. G. Hu, H. H. Cheng, Y. Hu, Z. P. Zhang, G. Q. Shi and L. T. Qu, *Adv. Mater.*, 2013, **25**, 2326–2331.
- 9 H. Sun, X. M. Fu, S. L. Xie, Y. S. Jiang and H. S. Peng, *Adv. Mater.*, 2016, **28**, 2070–2076.
- 10 T. Chen, R. Hao, H. S. Peng and L. M. Dai, *Angew. Chem., Int. Ed.*, 2015, **54**, 618–622.
- 11 D. S. Yu, K. L. Goh, Q. Zhang, L. Wei, H. Wang, W. C. Jiang and Y. Chen, *Adv. Mater.*, 2014, **26**, 6790–6797.
- 12 Q. H. Meng, H. P. Wu, Y. N. Meng, K. Xie, Z. X. Wei and Z. X. Guo, *Adv. Mater.*, 2014, **26**, 4100–4106.
- 13 L. Kou, T. Q. Huang, B. N. Zheng, Y. Han, X. L. Zhao, K. Gopalsamy, H. Y. Sun and C. Gao, *Nat. Commun.*, 2014, **5**, 3754.
- 14 G. Z. Sun, X. Zhang, R. Z. Lin, J. Yang, H. Zhang and P. Chen, *Angew. Chem., Int. Ed.*, 2015, **54**, 4651–4656.
- 15 Y. F. Luo, Y. Zhang, Y. Zhao, X. Fang, J. Ren, W. Weng, Y. S. Jiang, H. Sun, B. J. Wang, X. L. Cheng and H. S. Peng, *J. Mater. Chem. A*, 2015, **3**, 17553–17557.
- 16 Z. An, O. C. Compton, K. W. Putz, L. C. Brinson and S. T. Nguyen, *Adv. Mater.*, 2011, **23**, 3842–3846.
- 17 Y. Y. Zhang, Y. C. Li, P. Ming, Q. Zhang, T. X. Liu, L. Jiang and Q. F. Cheng, *Adv. Mater.*, 2016, **28**, 2834–2839.
- 18 Q. F. Cheng, M. X. Wu, M. Z. Li, L. Jiang and Z. Y. Tang, *Angew. Chem., Int. Ed.*, 2013, **52**, 3750–3755.
- 19 S. J. Wan, Y. C. Li, J. S. Peng, H. Hu, Q. F. Cheng and L. Jiang, *ACS Nano*, 2015, **9**, 708–714.
- 20 K. Gopalsamy, Z. Xu, B. N. Zheng, T. Q. Huang, L. Kou, X. L. Zhao and C. Gao, *Nanoscale*, 2014, **6**, 8595–8600.
- 21 G. Z. Sun, J. Q. Liu, X. Zhang, X. W. Wang, H. Li, Y. Yu, W. Huang, H. Zhang and P. Chen, *Angew. Chem., Int. Ed.*, 2014, **53**, 12576–12580.
- 22 F. K. Meng, J. T. Li, S. K. Cushing, M. J. Zhi and N. Q. Wu, *J. Am. Chem. Soc.*, 2013, **135**, 10286–10289.
- 23 S. Cheng, X. Chen, Y. G. Hsuan and C. Y. Li, *Macromolecules*, 2012, **45**, 993–1000.
- 24 J. Wang, J. L. Liu, D. L. Chao, J. X. Yan, J. Y. Lin and Z. X. Shen, *Adv. Mater.*, 2014, **26**, 7162–7169.
- 25 D. S. Yu, K. Goh, H. Wang, L. Wei, W. C. Jiang, Q. Zhang, L. M. Dai and Y. Chen, *Nat. Nanotechnol.*, 2014, **9**, 555–562.
- 26 K. Q. Zhou, S. H. Jiang, C. L. Bao, L. Song, B. B. Wang, G. Tang, Y. Hu and Z. Gui, *RSC Adv.*, 2012, **2**, 11695–11703.
- 27 Z. L. Dong, C. C. Jiang, H. H. Cheng, Y. Zhao, G. Q. Shi, L. Jiang and L. T. Qu, *Adv. Mater.*, 2012, **24**, 1856–1861.
- 28 G. Xin, T. Yao, H. Sun, S. M. Scott, D. Shao, G. Wang and J. Lian, *Science*, 2015, **349**, 1083–1087.
- 29 Z. Xu, Z. Liu, H. Y. Sun and C. Gao, *Adv. Mater.*, 2013, **25**, 3249–3253.
- 30 E. Frackowiak and F. Beguin, *Carbon*, 2001, **39**, 937–950.
- 31 P. Simon and Y. Gogotsi, *Nat. Mater.*, 2008, **7**, 945–954.
- 32 P. Xu, T. Gu, Z. Cao, B. Wei, J. Yu, F. Li, J.-H. Byun, W. Lu, Q. Li and T.-W. Chou, *Adv. Energy Mater.*, 2014, **4**, 1300759.
- 33 Y. Ma, P. Li, J. W. Sedloff, X. Zhang, H. Zhang and J. Liu, *ACS Nano*, 2015, **9**, 1352–1359.